In situ measurement of CO_2 and CH_4 from aircraft over northeast China and comparison with OCO-2 data

Xiaoyu Sun[1,2], Minzheng Duan[*1,2,3], Yang Gao[4], Rui Han[2,5], Denghui Ji[1,2], Wenxing Zhang[1], Nong Chen[6], Xiangao Xia[1,2], Hailei Liu[3], Yanfeng Huo[7]

[1]LAGEO, Institute of Atmospheric Physics, Chinese Academy of Sciences, 100029 Beijing, China
[2]College of Earth and Planetary Sciences, University of Chinese Academy of Sciences, Beijing,100049, China
[3]Chengdu University of Information Technology, Chengdu, 610225, China,
[4]China Meteorological Administration, Beijing, 100089, China
[5]ICCES, Institute of Atmospheric Physics, Chinese Academy of Sciences, Beijing, 100029, China
[6]Heilongjiang Meteorological Bureau, Harbin, 150001, China
[7]Anhui Meteorology Service, Hefei, 230061, China

Corresponding to: Minzheng Duan (dmz@mail.iap.ac.cn)

Abstract. Several satellites have been launched to monitor the increasing concentrations of greenhouse gases, especially CO_2 and CH_4 in the atmosphere, through back-scattered hyperspectral radiance in the shortwave infrared (SWIR) band. The vertical profiles of greenhouse gases and aerosols could strongly affect the results from these instruments. To investigate the effects of the vertical distribution of CO_2 on the uncertainty of SWIR satellite retrieval results, we conducted observations of the vertical profiles of CO_2, CH_4, and aerosol particles at 0.6–7 km above sea level using a Beechcraft King Air 350ER in Jiansanjiang (46.77°N, 131.99°E), Heilongjiang province, Northeast China, on 7-12 August, 2018. The profiles from this aircraft captured a decrease in CO_2 from 2 km to the minimum altitude due to the absorption of vegetation at the surface in summer. CH_4 measurements showed about 0.2 ppm increase from 2.0 to 0.6 km in 10 August, which may result from emissions from the large area of paddy fields below, and a constant mole fraction between 1.951 and 1.976 ppm was recorded at 2 km and above in three days. Comparison of CO_2 profiles from a new version of the carbon cycle data assimilation system Tan-Tracker (v1), retrievals from OCO-2 and aircraft measurements was conducted. The results from OCO-2 and the assimilation model system Tan-Tracker captured the vertical structure of CO_2 above 3 km, whereas below 3 km, the values from OCO-2 and Tan-Tracker model were lower than those from in situ measurements. Column-averaged CO_2 volume mole fractions calculated from in situ measurements showed biases of -4.68 ± 0.44 ppm ($-1.18\% \pm 0.11\%$) compared to OCO-2 retrievals.

1 Introduction

Global warming due to greenhouse gases (GHGs) has become one of the most urgent and widely studied issues in recent years. The Fifth Assessment Report of the Intergovernmental Panel on Climate Change (IPCC) noted that the global average temperature has increased by 0.85℃ over the period of 1880–2012. GHGs, especially the increasing CO_2 levels in the atmosphere related to anthropogenic activities, are blamed for global warming, because they absorb and emit radiant energy

within the thermal infrared range. Emission of CO_2 from fossil fuel combustion and industrial processes has contributed about 78% of the total GHG emissions increase from 1970 to 2010 (IPCC, 2015). Accurate measurement of CO_2 concentrations and their spatial and temporal variations in the atmosphere is essential for estimation of sources and sinks in regional and global

35   models (Patra et al., 2005a, 2005b; Zhang et al., 2008). The Global Atmospheric Watch program (http://www.wmo.int/gaw) coordinates the systematic observation and analysis of GHGs and other trace substances, providing an important source of local and global GHG data. However, ground-based and in situ measurements near the surface can only provide information about the lower atmosphere, and are insufficient for analysis of total-column GHGs, which exhibits variations in both vertical and horizontal directions. Over the past few years, several satellites, including the Greenhouse Gases Observing Satellite

40   (GOSAT, launched in January 2009), Second Orbiting Carbon Observatory, (OCO-2, launched in 2014), and TanSat (launched in 2016), have been launched into space to monitor CO_2 by observing back-scattered hyperspectral radiance in shortwave infrared (SWIR) wavelength, which can provide global coverage of the column-averaged dry-air mole fraction of CO_2 (X_{CO2}). Studies have shown that, given a 1–2 ppm accuracy of X_{CO2}, the use of space-borne instrument data can reduce the uncertainties in regional ($8° \times 10°$ footprint) estimation of CO_2 sources and sinks (Rayner and O'Brien, 2001). In addition, CO_2 vertical

45   profiles in the 5–25 km altitude range can be obtained using limb viewing space-borne sounders such as the Atmospheric Chemistry Experiment Fourier Transform Spectrometer (ACE-FTS, launched in August 2003). Foucher et al. (2009) reported the feasibility and difficulty of obtaining vertical CO_2 profiles using this method.

To validate and calibrate the X_{CO2} data from satellite measurement products, the Total Carbon Column Observing Network (TCCON), a network of ground-based solar Fourier transform spectrometers operating in the SWIR spectral region was

50   established (Wunch et al., 2011). Several studies have been conducted to determine the column-averaged volume mole fraction of CO_2, CH_4 and other trace gases (X_{CO2}, X_{CH4}, and X_{gas}) from TCCON data, which have shown good accuracy (Hedelius et al., 2017; Mendonca et al., 2019). In addition, commercial mobile solar-viewing near-infrared spectrometers of lower resolution than the TCCON instruments, such as Bruker^{TM} EM27/SUN, show potential for measurement of X_{gas} with an acceptable bias (Hedelius et al., 2016).

55   Retrieval accuracy is affected by knowledge of the vertical distribution of aerosols and CO_2. Vertical profiles of CO_2 also affect the accuracy of estimation for regional carbon fluxes in atmospheric transport model, and can help elucidate the global carbon cycle and climate change. Many experiments have been conducted to measure the vertical profiles of CO_2, CH_4, and other trace gases. The AirCore sampling system can be used to obtain vertical profiles of CO_2 and CH_4 from near the surface to 8–12 km with high accuracy (Karion et al., 2010; Membrive et al., 2017). Active remote sensing of atmospheric X_{CO2} with

60   the Raman lidar (light detection and ranging) technique has been developed and used to measure CO_2 vertically in the troposphere (Zhao et al., 2007; Gong et al., 2013; Han et al., 2017). CO_2 concentrations were measured at 8–12 km by Tohoku University (Sendai, Japan) through flask sampling on a commercial airliner operated by Japan Airlines (JAL) between Japan and Australia in 1984 and 1985 (Nakazawa et al., 1991). The Comprehensive Observation Network for TRace gases by AIrLiner (CONTRAIL) project installed continuous CO_2 measurement equipment onboard aircraft operated by JAL for in situ

65   measurement (Machida et al., 2008). The data for CONTRAIL are collected at altitudes between a few kilometers and 10 km,

taking advantage of the frequent movement of commercial aircraft around the world. The Civil Aircraft for Remote Sensing and In Situ Measurements Based on the Instrumentation Container Concept (CARIBIC) project (Brenninkmeijer et al., 1999; Brenninkmeijer et al., 2007) aimed to observe trace gases such as CO, O_3, and CO_2 by deploying measurement equipment in passenger aircraft. The HIAPER Pole-to-Pole Observation (HIPPO) project involved a sequence of five global aircraft

70 measurement programs to sample the atmosphere from near the North Pole to the coastal waters of Antarctica (Wofsy, 2011). Direct measurements that are independently collected from the aircraft provide validation information for satellite products. Several studies have shown that profile measurements of CO_2 and CH_4 obtained using aircraft and AirCore are useful for bias correction of both TCCON measurements (Deutscher et al., 2010; Hedelius et al., 2016) and satellite products (Araki et al., 2010; Inoue et al., 2013, 2014; Miyamoto et al., 2013; Frankenberg et al., 2016; Wunch et al., 2017).

75 Three satellites designed for CO_2 measurement, TanSAT (Yang et al., 2018; Yang et al., 2020), GMI/GF-5 (Li et al., 2016), and GAS/FY-3D (Qi et al., 2020), were launched into space in 2016, 2017, and 2018, respectively. Measurement of profiles is crucial to further validating the retrieved hyperspectral measurements from these three satellites. Because the algorithm for satellite retrieval requires *a priori* profiles based on the model and in situ measurements, the lack of direct and independent airborne observations may increase the bias in the satellite results over China.

80 In this study, in situ aircraft-based measurements of CO_2 and CH_4 were conducted in Jiansanjiang, Northeast China, in August 2018. An ultraportable greenhouse gas analyzer (UGGA; model 915-0011; Los Gatos Research, San Jose, CA, USA) was used onboard the aircraft to measure the vertical mole fractions of CO_2 and CH_4 at altitudes of 0.6–7 km. Descriptions of the aircraft, the onboard instruments and the OCO-2 and Tan-tracker data used in the paper are provided in Section 2. Details of the experimental site and the flight trajectory are provided in Section 3. The data processing method including the water vapour

85 correction is given in Section 4. A comparison of the profiles obtained using aircraft with OCO-2 and the assimilation system Tan-Tracker (v1) is described in Section 5. The methods used to calculate X_{CO2} and extrapolate in situ profiles, as well as error estimation, are discussed in Section 6.

2 Methods

2.1 Aircraft Instrumentation

90 The aircraft used for this experiment was a Beechcraft King Air 350ER, which is a twin-turboprop aircraft designed for weather modification missions and measurement of trace gases and aerosols by the China Meteorological Administration (CMA). The cruising speed and maximum speed of the aircraft are 441 and 561 km/h, respectively. Temperature, wind speed, relative humidity, and other meteorological data were detected and recorded by an Aircraft Integrated Meteorological Measurement System (AIMMS-20AG) installed on the aircraft. The geolocation information including latitude, longitude, ambient pressure

95 and height of the aircraft is also measured by AIMMS-20AG. The relative humidity is calculated by temperature and dew point, measured by the Total Temperature Sensor (Model 102 Type Non-De-iced, Rosemount Aerospace Inc) and Dew Point Hygrometer (Model 137 Vigilant™, EdgeTech), respectively.

The ultraportable greenhouse gas analyzer, UGGA (model 915-0011; Los Gatos Research), was connected to an aircraft-based impactor inlet system which consists of CVI (Model 1204; Brechtel Manufacturing Inc.) and ISO inlet (Model 1200; Brechtel Manufacturing Inc.) in the pressurized cabin for continuous measurement of CO_2 and CH_4. The CVI and/or ISO inlets were mounted on the top of the aircraft body as shown in Figure 1, and the air flow rate of the inlets was kept constant by the automatic air flow controller of the inlets (Aircraft-based Counterflow Virtual Impactor Inlet System CVI - Model 1204, Brochure; Isokinetic Inlet System ISO Inlet - Model 1200, Brochure). The UGGA uses a laser absorption technology called off-axis integrated cavity output spectroscopy to determine the trace gas concentration with a high precision of < 300 ppb (CO_2) and < 2 ppb (CH_4) and a 10-s response time (UGGA user manual, model 915-0011; Los Gatos Research) and was tested and controlled in the laboratory. As shown in the in-flight schematic diagram (Figure 1), the external oil-less diaphragm vacuum pump (F-9A 08-03, GAST) was mounted between the CVI inlet and/or the ISO inlet, and well-designed to keep a stable airflow with the maximum flow rate of 31.15 lpm (litter per minute). The ISO inlet was used as the aircraft pass through clouds, and CVI inlet was used in the other times. Similar system for airborne GHG measurement has been reported by O'Shea et al. (2013) and Palmer et al. (2013).

During the flight, the pressure of the sample cavity was kept constant by a small pump inside the instrument with the airflow about 0.3 lpm. The sample cavity temperature was also kept stable and constant by the temperature controller of the instrument. The instrument automatically recorded and saved the temperature and pressure in the cavity during operation. According to the records, the standard deviation of the cell pressure during three flights is 0.029, 0.029, 0.033 on 7, 9 and 10 August and the range of the cell pressure on each flight is below 0.12 torr. For the cell temperature, the standard deviation is 0.46, 1.55 and 1.18 on each day and the range is below 3.11℃. The UGGA was calibrated against standard GHGs (provided by the National Institute of Metrology, China) before take-off and after landing of each flight to ensure the accuracy of the data measured with the UGGA. Before this study, the GHG standard gases have been used by the CMA, Chinese Academy of Sciences, and other scientific research institutions for calibration and validation, showing that these standard gases have good performance and reliability. The standard gas we used is based on dry and clean air with known concentration values, filled in a 29.5L aluminium alloy cylinder with silanization and other special treatment on the inner wall, traceable to the world meteorological organization global atmospheric observation network (WMO-GAW) level 1 standard gas. The concentration of the CO_2 is 400.13 ppm and CH_4 is 1.867 ppm. The standard gas has been measured in the laboratory for the proportion of δ13C in CO_2, the proportion is between -8.0‰ and -8.2‰, close to the natural content, so it will not cause significant isotopic effect on the measurement of CO_2 by optical method and meet the requirements of standard gas (Yao et al., 2013). Just before taking off, UGGA was calibrated against standard gas, and the stability of instrument was checked and tested again using the same standard gas of CO_2 and CH_4 immediately after landing. As shown in Figure 2, the concentration of CO_2 and CH_4 before and after landing is stable around the values of standard gas concentration, and there was almost no drift after the flight. The precision and repeatability of the instruments are also checked and tested multiple times in laboratory and the results show that it is stable and good for the measurements.

2.2 Tan-Tracker and OCO-2 data

Based on the nonlinear least squares four-dimensional variational data assimilation algorithm (NLS-4DVar) and the Goddard Earth Observing System atmospheric chemistry transport model (GEOS-Chem), Tan-Tracker provides surface flux inversion estimates and profiles of CO_2 with 47 levels of vertical resolution from the surface to 0.03 hPa and horizontal resolution of
135 $2.5° \times 2°$. The NLS-4DVar assimilation model Tan-Tracker (v1) and OCO-2 X_{CO2} (v9r) retrievals are used to optimize surface terrestrial ecosystem CO_2 flux and ocean CO_2 flux, while prior fossil fuel emission and fire emission remain unchanged (details of model setting and prior flux information can be found in Han and Tian, 2019).

The Orbiting Carbon Observatory-2 (OCO-2), successfully launched on 2 July 2014, obtained global measurement of CO2 through hyperspectral measurement of reflected sun light from earth atmosphere in one NIR and two SWIR bands centre at
140 0.76, 1.61 and 2.06 µm, more details about the mission, retrieving algorithm and data characteristic can be found in Crisp et al. (2008) and O'Dell et al. (2012). The uncertainty and bias of the X_{CO2} products related to surface properties, aerosol and cloud, and the retrieving algorithm has been reported by Butz et al. (2009), Jung et al. (2016) and Connor et al. (2016). The OCO-2 data (V9r) including X_{CO2}, CO_2 profile and the *a priori* profile were used in this study.

3 Experimental Site

145 Aircraft measurement were carried out from 7 to 10 August over Jiansanjiang (47.11°N, 132.66°E, 61 m above sea level), located in Heilongjiang province, Northeast China. Figure 3 shows the geolocation of the Jiansanjiang aircraft and the flight paths. The area is mostly covered with large tracts of farmland. Rice cultivation is carried out primarily in summer, and crop growth is vigorous during this period. Due to the influence of plant photosynthesis, a large amount of CO_2 uptake occurs near the surface.

150 Three profiles were obtained between around 08:00 and 11:00 in local time (GMT+8) on 7, 9 and 10 August, 2018. The aircraft is designed for weather modification by China Meteorological Administration (CMA), so the infrastructure of the aircraft and the gas flow system are also designed and completed in the USA by the team of weather modification agency. CMA is in charge of the flight route, and there is a chance (several times later are planning) that it can carry the greenhouse gas analyzer to measure the profiles of CO_2 and CH_4. The greenhouse gas analyzer was loaded on the aircraft and some parts
155 of air flow arrangements were modified to better fit the requirement for profile measurement. Due to the logistical problem and the ATC restriction, we must fly in the morning from around 7:30 to 11:00 (local time) of these days to avoid obstructing civil aviation. The details of the three flights are listed in Table 1.

The flight trajectory on 7 August is shown in Figure 4. The aircraft climbed up quickly and directly to the maximum height about 7.1 km 30 minutes after taking off, and then descended down step by step at about every 300 m. Since the 3-D figures
160 in these three days look identical, the flight trajectoriesy of the other two days (9 and 10 August) is not shown in Figure 4. Considering the sensitivity of the UGGA response, measurements during the ascent were discarded due to the rapid changes in air pressure, and only data collected while spiralling downward were regarded as valid and analyzed further. Data recorded

below 0.6 km were also rejected because samples were easily contaminated with exhaust emissions during the slowing and descent of the aircraft before landing. The spiral descent of the aircraft lasted about 2.5 h on the three days, and the number of effective layers of measurements are 17, 21 and 20, respectively, in 7, 9 and 10 August.

4 Data Processing

4.1 Water vapor correction

The mole fraction of CO_2 or CH_4 measured during flight is the volume in proportion to the air containing water vapor, which cannot be directly compared with values from other data sources due to different water vapor contents of the sampled air. Therefore, the effect of water vapor is corrected and the mole fractions of CO_2 and CH_4 to dry air are given by:

$$f_{gas\_dry} = \frac{f_{gas} \cdot p}{p - p_{H_2O}}$$ (1)

where f_{gas_dry} (mol/mol) is the mole fraction of a gas in dry air, and f_{gas} (mol/mol) is the measured mole fraction of a gas under the real air conditions with water vapor. P_{H_2O} is water vapor pressure in hPa, which can be calculated as:

$$p_{H_2O} = e_s \cdot RH$$ (2)

where e_s (hPa) is the saturated water vapor pressure at temperature T (K) at aircraft altitudes, which can be derived from the Clausius–Clapeyron equation (Wallace and Hobbs, 2006):

$$\ln \frac{e_s}{6.11} = \frac{L_v M_w}{R} (\frac{1}{273} - \frac{1}{T}) \approx 5.42 \times 10^3 (\frac{1}{273} - \frac{1}{T}).$$ (3)

where $L_v = 2.500 \times 10^6$ J Kg^{-1}, $M_w = 18.016$, which is the molecular weight of water, R = 8.3145 J $K^{-1}mol^{-1}$, and e_s (in hPa) at temperature T (in K). Pressure p (hPa) of the ambient atmosphere are measured by the aircraft meteorology system, AIMMS-20AG, and the temperature T (K) was measured by Total Temperature Sensor (Model 102 Type Non-De-iced). The relative humidity RH (%) was calculated by the dew point and temperature. The dew point data is obtained by Dew Point Hygrometer (Model 137 Vigilant™, EdgeTech).

4.2 Accuracy and precision

Before the aircraft take-off, the clocks of the UGGA, AIMMS-20AG, the Total Temperature Sensor and other instruments were adjusted to match those of the CO_2, CH_4, and weather system measurements, synchronizing these data to the altitude and geolocation of the aircraft. The data from UGGA and synchronous meteorology measurements, including temperature, pressure, and humidity of ambient atmosphere, are recorded every second, then smoothed with a 10-s running average to further remove errors caused by temporal mismatch considering the response time of the UGGA. Because the flights followed the spiral trajectories that descended approximately every 300 m, only data collected during level flight were retained and analyzed, whereas data from the descent periods were removed to avoid the effects from vertical variations in sampling during

rapid descent. The time points at the beginning and end of level flight are determined according to the altitude and its variation of the aircraft. Considering the residual time of the GHG measurement system, the data obtained 220s from the start of the level flight is considered to be observed when the aircraft is descending rather than in level, which may cause uncertainty of the measurement. Therefore, the data were kept after the level flight starting for 220s. If the duration time of certain level flight lasted less than 220s, the data observed during that level flight were also discarded.

The instrument was calibrated against the standard gas before and after each flight. All of the measurements during the calibration process, including the standard gas used for calibration can trace back to WMO scale. The maximum and the average values of the difference between the standard gas and the measurement of the instrument of each day was considered as the accuracy of the aircraft data. For the precision, noted that the instrument was not continuously calibrated against the standard gas during the flight, we calculated the one standard deviation of the data in each level flight, and the maximum of the average value of 1-σ on each day is considered as the precision of the aircraft measurement. The accuracy of CO_2 and CH_4 is below 0.66 ppm and 0.002 ppm, 0.16% and 0.10% of the CO_2 and CH_4 concentration in standard gas, respectively. For precision, the 1-σ value is below 0.71 ppm and 0.0062 ppm for CO_2 and CH_4, respectively.

5 Results and Discussion

5.1 CO_2 and CH_4 profiles

Figure 5 shows vertical profiles of the CO_2 and CH_4 mole fractions measured with the UGGA during the flight over Jiansanjiang, which is an agricultural area that produces a large amount of rice. The CO_2 concentration increased with height in the troposphere (Figure 5a), which may result from CO_2 uptake by rice plants near the surface during the summer growth season. The greater increase rate of CO_2 in the lower troposphere on 7 August compared to the other two days was probably attributed to differing weather conditions on the three sampling days. 7 August was a sunny day, but it was overcast on 9 and 10, August, which may have weakened photosynthesis in rice and reduced CO_2 uptake. During all three flights, the maximum mole fraction of CO_2 reached about 418 ppm in the free troposphere at the top of the profile.

The mole fraction of CH_4 (Figure 5b) showed a consistent decrease with increasing altitude, ranging from 1.95 to 2.10 ppm from about 2 km to near the surface, possibly as a result of CH_4 emissions from agricultural activity at the surface. CH_4 showed low variability of less than 0.5 ppm at higher altitudes, from above 2 to 7 km, indicating a well-mixed vertical structure of CH_4 in the free troposphere.

Comparing the CO_2 and CH_4 observation data, the mole fraction of CH_4 varied less than that of CO_2 from 1.5–2 km up to the free troposphere, with a stable value of about 1.925 ppm, indicating that CH_4 was evenly mixed at these heights and there were no obvious sources or sinks of CH_4. While CO_2 increase with altitude in the free troposphere from about 400 to 418 ppm. This increase may have been due to photosynthesis by vegetation and the large number of crops planted locally, creating a CO_2 sink at the surface, and causing the CO_2 concentration to rise with height in the free troposphere. The results show that

the vertical profile of CO_2 in summer increases with height in the upper troposphere, whereas that of CH_4 changed little with height and was relatively stable over Jiansanjiang area during experiment.

5.2 Comparison of profiles from the model and satellite product

Aircraft measurements were compared with CO_2 data obtained from OCO-2 (v9r) retrievals and the recently developed data assimilation system for the global carbon cycle, Tan-Tracker (v1) (Han and Tian, 2019). The assimilation data are collected and linearly interpolated spatially and temporally based on the geolocation of the observation site and time. Because no data were obtained from OCO-2 (v9r) over Jiansanjiang during the flight, the results of OCO-2 within $1° \times 1°$ spatially at the closest time to the flight were used for comparison, which were collected on 5 August. The height of the profile is available on the satellite product.

The structure of CO_2 varying with height could be roughly divided into three segments: surface to 2 km, 2 to 3 km, and 3 to 8 km (Figure 6). Below 2 km, CO_2 of Tan-tracker model is assumed to be well mixed and uniformly distributed with height, with values ranging from 385 to 395 ppm, therefore, the model could not reproduce the strong decrease in CO_2 from 2 km to the surface due to uptake by vegetation. From 2 to 3 km, CO_2 increased to about 400 ppm with altitude. The averaged satellite retrieval profiles correctly reproduced the decrease in CO_2 from 2 km to the surface, but the decrease rate was lower than those of in situ profiles, decreasing from 393 ppm at 2 km to 390 ppm near the surface. Flight data showed a significant CO_2 sink in this region, most notably on 7 August when it decreased from 400 ppm at 2 km to 380 ppm at 0.6 km. The impact of ground sinks was more pronounced and apparent than that from satellite inversion and model simulations, indicating that the strong variations in the lower atmosphere and planetary boundary layer (PBL) should be more carefully considered in model and retrieval algorithms. Between 2 and 4 km, aircraft profiles showed a relatively uniform mixing level of CO_2, with roughly stable concentrations around 400 ppm.

In general, all profiles from aircraft, satellite retrieval, and model showed a similar vertical distribution trend in the troposphere above 2 km, but with differences in values. The average of the difference between OCO-2 and the aircraft profiles above 2 km is 4.22 ppm, 8.16 ppm and -2.57 ppm in 7, 9 and 10 August, respectively. The volume mole fraction of CO_2 from both satellite and aircraft measurements indicated a CO_2 sink. GHGs profiles have rarely been observed before near the experiment site, or over Northeast of China as far as we know. The model simulations are based on data of regional emission inventory. The accuracy of simulated profiles and concentrations near surface over the experiment site still remains unknown. So continuous and regular observation of the GHGs profiles are necessary for better understanding of the regional emission amounts and the variation of the GHGs.

5.3 Comparison of X_{CO_2} products

The total column amount of CO_2, can be derived by integrating the CO_2 concentrations from the surface to the top of the atmosphere under the assumption of hydrostatic conditions:

$$VC_{CO_2} = \int_0^{P_s} \frac{f_{co_2}^{dry} \cdot (1 - f_{H_2O})}{g(p) \cdot m(p)} dp$$

$$m = [m_{H_2O} \cdot f_{H_2O} + m_{air}^{dry} \cdot (1 - f_{H_2O})]$$

(4)

where VC_{CO_2} is the total column amount of CO_2, $f_{co_2}^{dry}$ is the dry-air mole fraction (DMF) of CO_2 (mol mol^{-1}), $f_{H_2O}(p)$ is the aircraft profile of H_2O (mol mol^{-1}), which is measured by the onboard AIMMS system, $m(p)$ is the mean molecular mass of wet air, and $g(p)$ is gravitational acceleration, $m_{H_2O} = 18.02 \times 10^{-3}/N_A$ kg/molecule, $m_{air}^{dry} = 28.964 \times 10^{-3}/N_A$ kg/molecule, and N_A is Avogadro's constant. Data beyond the flight limits are taken from National Centers for Environmental Prediction (NCEP) reanalysis data interpolated to the time of flight.

The column-averaged DMF of CO_2 (X_{CO2}) from aircraft measurements was calculated based on the method of Wunch et al. (2010), which considers the average kernel in OCO-2 satellite retrievals:

$$X_{CO_2}^{in\ situ} = X_{CO_2}^a + \sum_j h_j a_j (t_{in\ situ} - t_a)_j$$

(5)

where a is the average kernel (Rodgers and Connor, 2003), $X_{CO_2}^a$ is the column-averaged DMF for the a priori profile t_a, h_j is the pressure weighting function of OCO-2, and $t_{in\ situ}$ is the in situ profile from aircraft measurement.

Because in situ measurements available from aircraft are limited, values outside the aircraft's vertical observation range must be estimated to calculate X_{CO2}. Two extrapolation methods were used to extend the profile of the aircraft measurements and then estimates the X_{CO2} value of the in-situ measurement respectively. 1) The unknown part of the aircraft profile was directly from the OCO-2 a prior profile. 2) A well-mixed and constant mixing ratio of CO_2 is assumed from the surface to the lower limit of flight, and from the upper limit of flight to the tropopause. The CO_2 concentrations above the tropopause were calculated with an empirical model (Toon and Wunch, 2014) which considers tropopause height as well as realistic latitude and time dependencies through curve fitting of data from high-altitude balloons, AirCore, Observations of the Middle Stratosphere balloon, and aircraft. In general, the mole fraction of CO_2 decreased exponentially with height from the tropopause to upper stratosphere, and the tropopause height was obtained from NCEP reanalysis data with a 2.5° × 2.5° resolution, which was linearly interpolated to the geographic coordinates of Jiansanjiang. Figure 7 shows the extrapolated CO_2 profiles using method (2).

X_{CO2} calculated from the aircraft measurements and differences with that from OCO-2 are listed in Table 2 and 3. The results showed that X_{CO2} values of OCO-2 were lower, with an average difference of −4.68 ± 0.44 ppm (−1.18% ± 0.11%) and -5.09 ± 1.28 ppm (-1.28% ± 0.32%) by method (1) and by method (2).

Uncertainties induced by extrapolation of profiles outside the height limits of aircraft and errors in tropopause estimation were analyzed. Errors in extrapolation of the profile below the lower limit and above the upper limit of flight were estimated by recalculating X_{CO2} after a 1-ppm positive shift in the CO_2 concentrations at these altitudes. For method (1), since the values of CO_2 mole factions of unknown part is the same as that of the OCO-2 a priori profile, as Eq. (5) shows, no extra uncertainty would be introduced by extrapolation. But for method (2), as the profile is assumed to decrease exponentially with height

above the tropopause, the height of the tropopause also introduces uncertainties for X_{CO2}. Table 4 lists the errors resulting from three sources: 1) uncertainties from in situ measurement, 2) extrapolation of the profile in the PBL where no in situ measurements were collected, and 3) profile assumptions above the upper limit of flight observations. Errors due to uncertainty in tropopause height were analyzed by shifting the tropopause height upward by 1 km, and the results are also listed in Table 4. These results indicated that the extrapolation method and assumptions used to construct profiles where no measurements were made were the primary source of errors, among which the greatest error was from the profile above the upper limit of the flight (0.323 ppm). Errors due to uncertainty in the tropopause height were also non-negligible. Because of the lack of observation data near the surface, the missing measurements were directly replaced by the data at the lowest altitude measured by the aircraft. The error caused by this practice is shown in Table 4, with an average of 0.079 ppm for X_{CO2}. This is also the impact of the lack of near-surface observations on X_{CO2} estimation. Therefore, observations from near the surface to about 1 km from other methods, such as in-situ GHG measurements by tethered balloon and high tower, are necessary for accurate estimation of X_{CO2}.

6 Conclusion

The vertical distributions of CO_2 and CH_4 were measured by using a Beechcraft King Air 350ER over Jiansanjiang, an extensive paddy area in Northeast China, and three vertical profiles from 0.6 to 7.5 km were obtained on 7, 9 and 10 August. Measurements of the mole fraction of CO_2 showed an increase with height, whereas CH_4 decreased with height. These results are reasonable, because paddies are sinks for CO_2 and sources of CH_4 during the summer growing season. Comparing the observed profiles from aircraft with those from the carbon cycle data assimilation system Tan-Tracker (v1) and OCO-2 retrievals showed that the general vertical structure was consistent, but the values of mole fraction of CO_2 from Tan-Tracker and OCO-2 had negative bias estimates. The average bias between aircraft and OCO-2 is -4.68 ± 0.44 ppm ($-1.18\% \pm 0.11\%$). The uncertainty mainly resulted from extrapolation of the profile beyond the flight limit, where no in situ measurements were available.

Data availability

Data used in this study are available from the corresponding author upon request (dmz@mail.iap.ac.cn).

Author contributions

M. Duan and X. Sun determined the main goal of this study. X. Sun carried it out, analyzed the data, and prepared the paper with contributions from all co-authors. Y. Gao and N. Chen provided technical guidance for related instrument.

305 **Competing interests**

The authors declare that they have no conflict of interests.

Acknowledgements

This work is supported by the National Natural Science Foundation of China (No. 41527806 and No.41705014). We also acknowledge numerous staff of the Weather Modification Center, China Meteorological Administration for supporting the
310 experiment and the instrumentation onboard the aircraft. We also thank Jiansanjiang Airport for providing the experimental site and arranging time for conducting the campaign.

References

Araki, M., Morino, I., Machida, T., Sawa, Y., Matsueda, H., Ohyama, H., Yokota, T., and Uchino, O.: CO 2 column-averaged volume mixing ratio derived over Tsukuba from measurements by commercial airlines, Atmos. Chem. Phys., 10, 7659-7667,
315 2010.

Brenninkmeijer, C., Crutzen, P., Boumard, F., Dauer, T., Dix, B., Ebinghaus, R., Filippi, D., Fischer, H., Franke, H., and Frieβ, U.: Civil Aircraft for the regular investigation of the atmosphere based on an instrumented container: The new CARIBIC system, Atmos. Chem. Phys., 7, 4953-4976, 2007.

Brenninkmeijer, C., Crutzen, P., Fischer, H., Güsten, H., Hans, W., Heinrich, G., Heintzenberg, J., Hermann, M., Immelmann,
320 T., and Kersting, D.: CARIBIC—Civil aircraft for global measurement of trace gases and aerosols in the tropopause region, J. Atmos. Ocean Technol., 16, 1373-1383, http://doi:10.1175/1520-0426(1999)016<1373:CCAFGM>2.0.CO;2, 1999.

Crisp, D., Miller, C. E., and DeCola, P. L.: NASA Orbiting Carbon Observatory: measuring the column averaged carbon dioxide mole fraction from space, J. Appl. Remote. Sens., 2, 023508, http://doi:10.1117/1.2898457, 2008.

Deutscher, N., Griffith, D., Bryant, G., Wennberg, P., Toon, G., Washenfelder, R., Keppel-Aleks, G., Wunch, D., Yavin, Y.,
325 and Allen, N.: Total column CO2 measurements at Darwin, Australia-site description and calibration against in situ aircraft profiles, Atmos. Meas. Tech., 2010. 2010.

Deutscher, N., Griffith, D., Bryant, G., Wennberg, P., Toon, G., Washenfelder, R., Keppel-Aleks, G., Wunch, D., Yavin, Y., Allen, N., Blavier, J.-F., Jiménez, R., Daube, B. C., Bright, A. V., Matross, D. M., Wofsy, S. C., and Park, S.: Total column CO2 measurements at Darwin, Australia-site description and calibration against in situ aircraft profiles, Atmos. Meas. Tech.,
330 3, 947-958, http://doi:10.5194/amt-3-947-2010, 2010.

Endresen, Ø., Sørgård, E., Behrens, H. L., Brett, P. O., and Isaksen, I. S.: A historical reconstruction of ships' fuel consumption and emissions, J. Geophys. Res. Atmos., 112, http://doi:10.1029/2006JD007630, 2007.

Foucher, P., Chédin, A., Dufour, G., Capelle, V., Boone, C., and Bernath, P.: Feasibility of CO 2 profile retrieval from limb viewing solar occultation made by the ACE-FTS instrument, Atmos. Chem. Phys., 9, 2873-2890, http://doi:10.5194/acp-9-
335   2873-2009, 2009.

Frankenberg, C., Kulawik, S. S., Wofsy, S. C., Chevallier, F., Daube, B., Kort, E. A., O'dell, C., Olsen, E. T., and Osterman, G.: Using airborne HIAPER Pole-to-Pole Observations (HIPPO) to evaluate model and remote sensing estimates of atmospheric carbon dioxide, Atmos. Chem. Phys., 16, 7867-7878, http://doi:10.5194/acp-16-7867-2016, 2016.

Geibel, M. C., Messerschmidt, J., Gerbig, C., Blumenstock, T., Chen, H., Hase, F., Kolle, O., Lavrič, J. V., Notholt, J., Palm,
340   M., Rettinger, M., Schmidt, M., Sussmann, R., Warneke, T., and Feist, D. G.: Calibration of column-averaged CH4 over European TCCON FTS sites with airborne in-situ measurements, Atmos. Chem. Phys., 12, 8763–8775, https://doi.org/10.5194/acp-12-8763-2012, 2012.

Gong, W., Han, G., Ma, X., and Lin, H.: Multi-points scanning method for wavelength locking in CO2 differential absorption lidar, Opt. Commun., 305, 180-184, http://doi:10.1016/j.optcom.2013.05.006, 2013.

345   Han, G., Ma, X., Liang, A., Zhang, T., Zhao, Y., Zhang, M., and Gong, W.: Performance evaluation for China's planned CO2-IPDA, Remote Sens., 9, 768, http://doi:10.3390/rs9080768, 2017.

Han, R. and Tian, X.: A dual-pass carbon cycle data assimilation system to estimate surface CO2 fluxes and 3D atmospheric CO2 concentrations from spaceborne measurements of atmospheric CO2, Geoscientific Model Development, doi: 10.5194/gmd-2019-54. http://doi:10.5194/gmd-2019-54.

350   Hedelius, J. K., Parker, H., Wunch, D., Roehl, C. M., Viatte, C., Newman, S., Toon, G. C., Podolske, J. R., Hillyard, P. W., Iraci, L. T., Dubey, M. K., and Wennberg, P. O.: Intercomparability of X_ (CO_2) and X_ (CH_4) from the United States TCCON sites, Atmos. Meas. Tech., 10, 1481-1493, http://doi:10.5194/amt-10-1481-2017, 2017.

Hedelius, J. K., Viatte, C., Wunch, D., Roehl, C. M., Toon, G. C., Chen, J., Jones, T., Wofsy, S. C., Franklin, J. E., Parker, H., Dubey, M. K., and Wennberg, P. O.: Assessment of errors and biases in retrievals of X CO 2, X CH 4, X CO, and X N 2 O
355   from a 0.5 cm–1 resolution solar-viewing spectrometer, Atmos. Meas. Tech., 9, 3527-3546, http://doi:10.5194/amt-9-3527-2016, 2016.

Inoue, M., Morino, I., Uchino, O., Miyamoto, Y., Saeki, T., Yoshida, Y., Yokota, T., Sweeney, C., Tans, P. P., Biraud, S. C., Machida, T., Pittman, J. V., Kort, E. A., Tanaka, T., Kawakami, S., Sawa, Y., Tsuboi, K., and Matsueda, H.: Validation of XCH 4 derived from SWIR spectra of GOSAT TANSO-FTS with aircraft measurement data, Atmos. Meas. Tech., 7, 2987-
360   3005, http://doi:10.5194/amt-7-2987-2014, 2014.

Inoue, M., Morino, I., Uchino, O., Miyamoto, Y., Yoshida, Y., Yokota, T., Machida, T., Sawa, Y., Matsueda, H., Sweeney, C. C., Tans P. P., Andrews A. E., Biraud S. C., Tanaka T., Kawakami S., and Patra, P. K.: Validation of XCO 2 derived from SWIR spectra of GOSAT TANSO-FTS with aircraft measurement data, Atmos. Chem. Phys., 13, 9771-9788, http://doi:10.5194/acp-13-9771-2013, 2013.

365   Jung, Y., Kim, J., Kim, W., Boesch, H., Lee, H., Cho, C., and Goo, T.-Y.: Impact of aerosol property on the accuracy of a CO2 retrieval algorithm from satellite remote sensing, Remote Sens., 8, 322, http://doi:10.3390/rs8040322, 2016.

Karion, A., Sweeney, C., Tans, P., and Newberger, T.: AirCore: An innovative atmospheric sampling system, J. Atmos. Ocean Technol., 27, 1839-1853, http://doi:10.1175/2010JTECHA1448.1, 2010.

Keller, C. A., Long, M. S., Yantosca, R. M., Da Silva, A., Pawson, S., and Jacob, D. J.: HEMCO v1. 0: a versatile, ESMF-compliant component for calculating emissions in atmospheric models, Geosci. Model Dev., 7, http://doi:10.5194/gmd-7-1409-2014, 2014.

Li, Y., Zhang, C., Liu, D., Chen, J., Rong, P., Zhang, X., and Wang, S.: CO_2 retrieval model and analysis in short-wave infrared spectrum, Optik., 127, 4422-4425, http://doi:10.1016/j.ijleo.2016.01.144, 2016.

Machida, T., Matsueda, H., Sawa, Y., Nakagawa, Y., Hirotani, K., Kondo, N., Goto, K., Nakazawa, T., Ishikawa, K., and Ogawa, T.: Worldwide measurements of atmospheric CO_2 and other trace gas species using commercial airlines, J. Atmos. Ocean Technol., 25, 1744-1754, http://doi:10.1175/2008JTECHA1082.1, 2008.

Membrive, O., Crevoisier, C., Sweeney, C., Danis, F., Hertzog, A., Engel, A., Bönisch, H., and Picon, L.: AirCore-HR: a high-resolution column sampling to enhance the vertical description of CH_4 and CO_2, Atmos. Meas. Tech., doi: amt-10-2163-2017, 2017. http://doi:amt-10-2163-2017, 2017.

Mendonca, J., Strong, K., Wunch, D., Toon, G. C., Long, D. A., Hodges, J. T., Sironneau, V. T., and Franklin, J. E.: Using a speed-dependent Voigt line shape to retrieve O_2 from Total Carbon Column Observing Network solar spectra to improve measurements of XCO_2, Atmos. Meas. Tech., 12, 35-50, http://doi:10.5194/amt-12-35-2019, 2019.

Messerschmidt, J., Geibel, M. C., Blumenstock, T., Chen, H., Deutscher, N. M., Engel, A., Feist, D. G., Gerbig, C., Gisi, M., Hase, F., Katrynski, K., Kolle, O., Lavrič, J. V., Notholt, J., Palm, M., Ramonet, M., Rettinger, M., Schmidt, M., Sussmann, R., Toon, G. C., Truong, F., Warneke, T., Wennberg, P. O., Wunch, D., and Xueref-Remy, I.: Calibration of TCCON column-averaged CO_2: the first aircraft campaign over European TCCON sites, Atmos. Chem. Phys., 11, 10765–10777, https://doi.org/10.5194/acp-11-10765-2011, 2011.

Miyamoto, Y., Inoue, M., Morino, I., Uchino, O., Yokota, T., Machida, T., Sawa, Y., Matsueda, H., Sweeney, C., Tans, P., Andrews, A. E., and Patra, P. K.: Atmospheric column-averaged mole fractions of carbon dioxide at 53 aircraft measurement sites, Atmospheric Chemistry & Physics Discussions, 12, http://doi:10.5194/acp-13-5265-2013, 2012.

Nakazawa, T., Miyashita, K., Aoki, S., and Tanaka, M.: Temporal and spatial variations of upper tropospheric and lower stratospheric carbon dioxide, Tellus., 43, 106-117, http://doi:10.1034/j.1600-0889.1991.t01-1-00005.x, 1991.

O'Brien, D. and Rayner, P.: Global observations of the carbon budget, 2, CO_2 column from differential absorption of reflected sunlight in the 1.61 μm band of CO_2, J. Geophys. Res. Atmos., 107, ACH 6-1-ACH 6-16, http://doi:10.1029/2001JD000617, 2002.

Oda, T. and Maksyutov, S.: A very high-resolution (1 km? 1 km) global fossil fuel CO_2 emission inventory derived using a point source database and satellite observations of nighttime lights, Atmos. Chem. Phys., 11, 543, http://doi:10.5194/acp-11-543-2011, 2011.

O'Dell, C., Connor, B., Bösch, H., O'Brien, D., Frankenberg, C., Castano, R., Christi, M., Fisher, B., Gunson, M., McDuffie, J., Miller, C. E., Natraj, V., Oyafuso, F., Polonsky, I., Smyth, M., Taylor, T., Toon, G. C., Wennberg, P. O., and Wunch, D.:

The ACOS CO2 retrieval algorithm-Part 1: Description and validation against synthetic observations, Atmos. Meas. Tech., 5, 99, http://doi:10.5194/amt-5-99-2012, 2012.

O'Shea, S., Bauguitte, S.-B., Gallagher, M., Lowry, D., and Percival, C.: Development of a cavity enhanced absorption spectrometer for airborne measurements of CH 4 and CO 2, Atmos. Meas. Tech., 6, http://doi:10.5194/amt-6-1095-2013, 2013.

Pachauri, R. K., Allen, M. R., Barros, V. R., Broome, J., Cramer, W., Christ, R., Church, J. A., Clarke, L., Dahe, Q., and Dasgupta, P.: Climate change 2014: synthesis report. Contribution of Working Groups I, II and III to the fifth assessment report of the Intergovernmental Panel on Climate Change, 151, 2014.

Palmer, P. I., Parrington, M., Lee, J. D., Lewis, A., Rickard, A., Bernath, P. F., Duck, T., Waugh, D., Tarasick, D., and Andrews, S.: Quantifying the impact of BOReal forest fires on Tropospheric oxidants over the Atlantic using Aircraft and Satellites (BORTAS) experiment: design, execution and science overview, Atmos. Chem. Phys., 13, http://doi:10.5194/acp-13-6239-2013, 2013.

Patra, P. K., Maksyutov, S., Ishizawa, M., Nakazawa, T., Takahashi, T., and Ukita, J. (2005a): Interannual and decadal changes in the sea-air CO2 flux from atmospheric CO2 inverse modeling, Global. biogeochem. cycles., 19, http://doi:10.1029/2004GB002257, 2005.

Patra, P. K., Ishizawa, M., Maksyutov, S., Nakazawa, T., and Inoue, G. (2005b): Role of biomass burning and climate anomalies for land-atmosphere carbon fluxes based on inverse modeling of atmospheric CO2, Global. biogeochem. cycles., 19, http://doi:10.1029/2004GB002258, 2005.

Pei-Tao, Z., Yin-Chao, Z., Lian, W., Yue-Feng, Z., Jia, S., Xin, F., Kai-Fa, C., Jun, X., and Xiao-Yong, D.: Analysis of influence of atmosphere extinction to Raman lidar monitoring CO2 concentration profile, Chin. Phys., 16, 2486, http://doi:10.1088/1009-1963/16/8/055, 2007.

Peters, W., Jacobson, A. R., Sweeney, C., Andrews, A. E., Conway, T. J., Masarie, K., Miller, J. B., Bruhwiler, L. M., Pétron, G., Hirsch, A. I., Worthy, D. E. J., Werf, G. R. v. d., Randerson, J. T., Wennberg, P. O., Krol, M. C., and Tans, P. P.: An atmospheric perspective on North American carbon dioxide exchange: CarbonTracker, Proc. Natl. Acad. Sci., 104, 18925-18930, http://doi:10.1073/pnas.0708986104, 2007.

Qi, C., Wu, C., Hu, X., Xu, H., Lee, L., Zhou, F., Gu, M., Yang, T., Shao, C., and Yang, Z.: High spectral infrared atmospheric sounder (HIRAS): system overview and on-orbit performance assessment, IEEE Trans. Geosci. Remote Sens., doi: 10.1109/TGRS.2019.2963085, 2020. http://doi:10.1109/TGRS.2019.2963085, 2020.

Randerson, J., van der Werf, G., Giglio, L., Collatz, G., and Kasibhatla, P.: Global Fire Emissions Database, Version 4,(GFEDv4), ORNL DAAC. 2015.

Rayner, P. and O'Brien, D.: The utility of remotely sensed CO2 concentration data in surface source inversions, Geophys. Res. Lett., 28, 175-178, http://doi:10.1029/2000GL011912, 2001.

Rodgers, C. D. and Connor, B. J.: Intercomparison of remote sounding instruments, J. Geophys. Res. Atmos., 108, http://doi:10.1029/2002JD002299, 2003.

435 Takahashi, T., Sutherland, S. C., Wanninkhof, R., Sweeney, C., Feely, R. A., Chipman, D. W., Hales, B., Friederich, G., Chavez, F., Sabine, C., Watson, A., C.E.Bakker, D., Schuster, U., Metzl, N., Yoshikawa-Inoue, H., Ishii, M., Midorikawa, T., Nojiri, Y., Körtzinger, A., Steinhoff, T., Hoppema, M., Olafsson, J., S.Arnarson, T., Tilbrook, B., Johannessen, T., Olsen, A., Bellerby, R., C.S.Wong, Delille, B., N.R.Bates, and Baar, H. J. W. d.: Climatological mean and decadal change in surface ocean pCO2, and net sea–air CO2 flux over the global oceans, Deep Sea Res. Part 2 Top. Stud. Oceanogr., 56, 554-
440 577, http://doi:10.1016/j.dsr2.2008.12.009, 2009.

Wallace, J. M. and Hobbs, P. V.: Atmospheric science: an introductory survey, Elsevier, 2006.

Wofsy, S. C.: HIAPER Pole-to-Pole Observations (HIPPO): fine-grained, global-scale measurements of climatically important atmospheric gases and aerosols, Philos. Trans. Royal Soc. A, 369, 2073-2086, http://doi:10.1098/rsta.2010.0313, 2011.

Wunch, D., Toon, G. C., Blavier, J.-F. L., Washenfelder, R. A., Notholt, J., Connor, B. J., Griffith, D. W., Sherlock, V., and
445 Wennberg, P. O.: The total carbon column observing network, Philos. Trans. Royal Soc. A, 369, 2087-2112, http://doi:doi.org/10.1098/rsta.2010.0240, 2011.

Wunch, D., Toon, G. C., Wennberg, P. O., Wofsy, S. C., Stephens, R. S., Fischer, M. K., Uchino, O., Abshire, J., Bernath, P., Biraud, S. C., Blavier, J.-F. L., Boone, C., Bowman, K. P., Browell, E. V., Campos, T., Connor, B. J., Daube, B. C., Deutscher, N. M., Diao, M., Elkins, J. W., Gerbig, C., Gottlieb, E., Griffith, D. W. T., Hurst, D. F., Jiménez, R., KeppelAleks,
450 G., Kort, E. A., Macatangay, R., Machida, T., Matsueda, H., Moore, F., Morino, I., Park, S., Robinson, J., Roehl, C. M., Sawa, Y., Sherlock, V., Sweeney, C., Tanaka, T., and Zondlo, M. A.: Calibration of the Total Carbon Column Observing Network using aircraft profile data, Atmos. Meas. Tech., doi: 10.5194/amt-3-1351-2010, 2010. http://doi:10.5194/amt-3-1351-2010, 2010.

Wunch, D., Wennberg, P. O., Osterman, G., Fisher, B., Naylor, B., Roehl, C. M., O'Dell, C., Mandrake, L., Viatte, C., and
455 Kiel, M.: Comparisons of the Orbiting Carbon Observatory-2 (OCO-2) X CO2 measurements with TCCON, Atmos. Meas. Tech., doi: 10.5194/amt-10-2209-2017, 2017. http://doi:10.5194/amt-10-2209-2017, 2017.

Yang, Z., Bi, Y.-M., Wang, Q., Liu, C.-B., Gu, S.-Y., Zheng, Y., Lin, C., Yin, Z., and Tian, L.: Inflight Performance of the TanSat Atmospheric Carbon Dioxide Grating Spectrometer, IEEE Trans. Geosci. Remote Sens., 2020. 2020.

Yang, Z., Zhen, Y., Yin, Z., Lin, C., Bi, Y., Liu, W., Wang, Q., Wang, L., Gu, S., and Tian, L.: Prelaunch radiometric
460 calibration of the tansat atmospheric carbon dioxide grating spectrometer, IEEE Trans. Geosci. Remote Sens., 56, 4225-4233, http://doi:10.1109/TGRS.2018.2829224, 2018.

Yao, B., Huang, J., Zhou, L., Fang, S., Liu, L., Xia, L., Li, P., and Wang, H.: Preparation of mixed standards for high accuracy CO2/CH4/CO measurements., Environ. Chem., 02, 135-140, http://doi:10.7524/j.issn.0254-6108.2013.02.019, 2013.

Yevich, R. and Logan, J. A.: An assessment of biofuel use and burning of agricultural waste in the developing world, Global.
465 biogeochem. cycles., 17, http://doi:10.1029/2002GB001952, 2003.

Zhang, D., Tang, J., Shi, G., Nakazawa, T., Aoki, S., Sugawara, S., Wen, M., Morimoto, S., Patra, P. K., and Hayasaka, T.: Temporal and spatial variations of the atmospheric CO2 concentration in China, Geophys. Res. Lett., 35, http://doi:10.1029/2007GL032531, 2008.
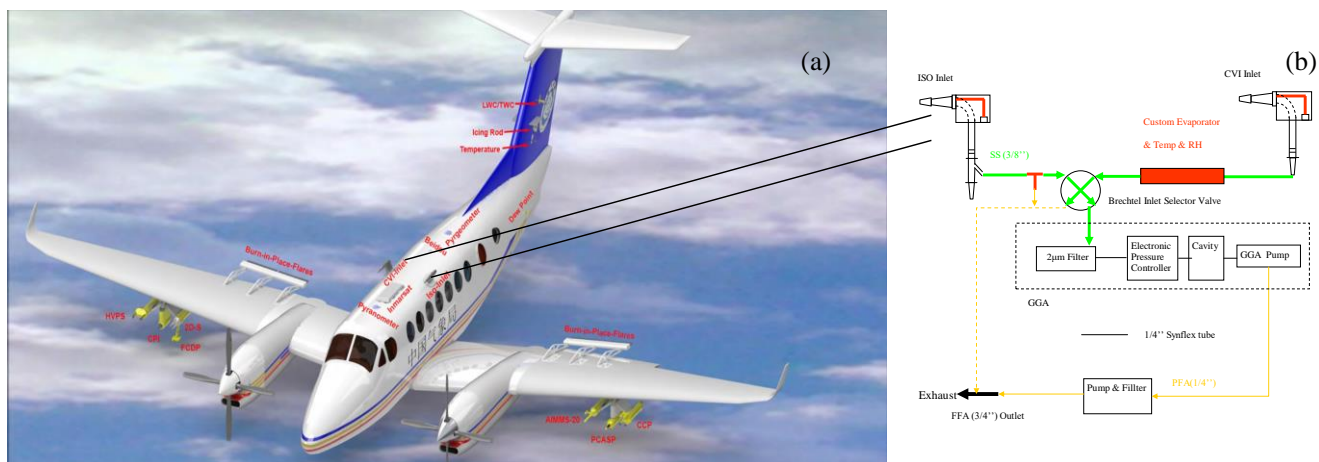
Figure 1. (a) The outside view of the Beechcraft King Air 350ER instrumentation. (b) The schematic diagram of the greenhouse gases sample airflow.
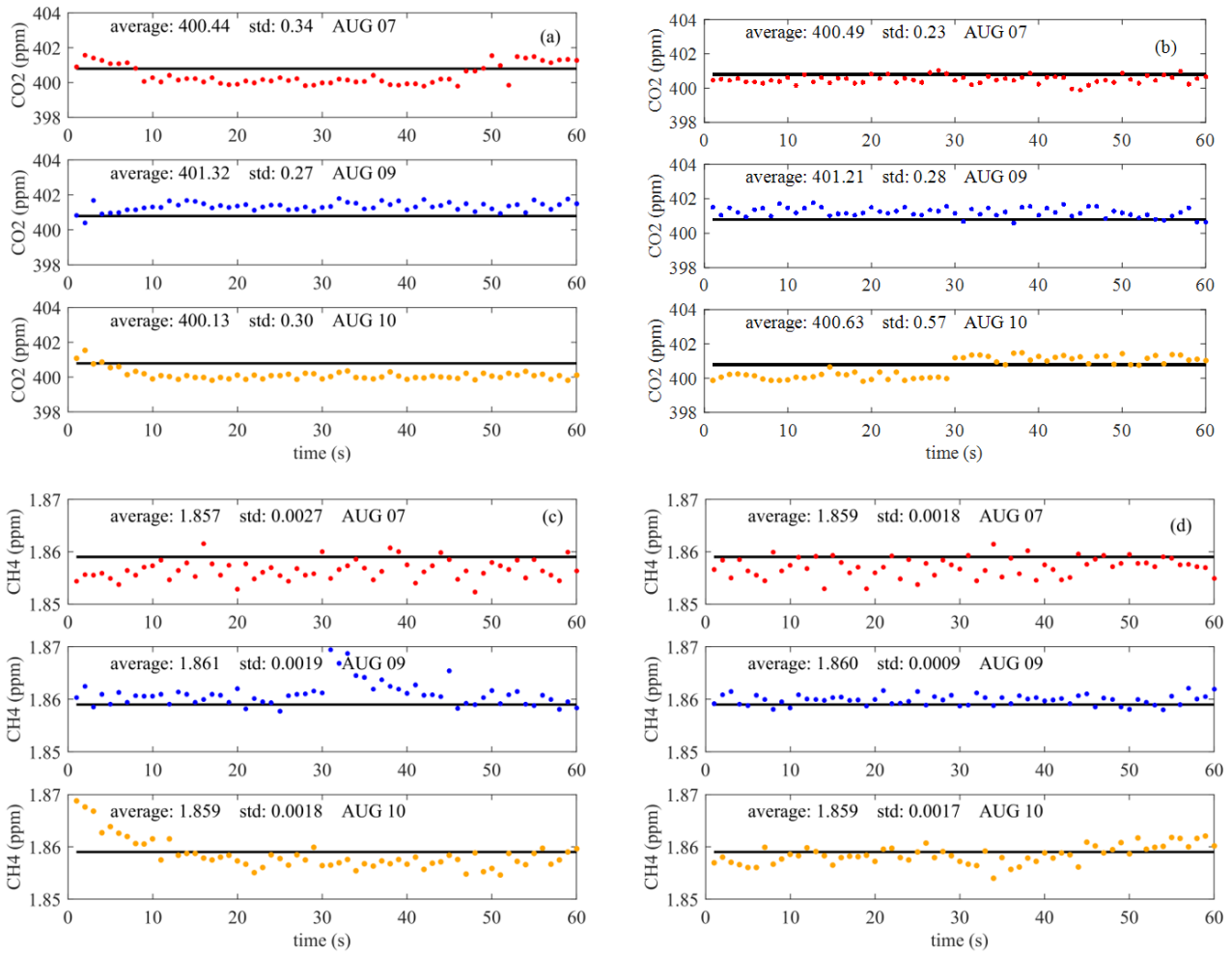
475 **Figure 2. The concentrations of CO₂ (a) and CH₄ (b) before the flight, and the concentrations of CO₂ (a) and CH₄ (b) after the flight obtained during the calibration, with the values of standard deviation and average of each calibration.**
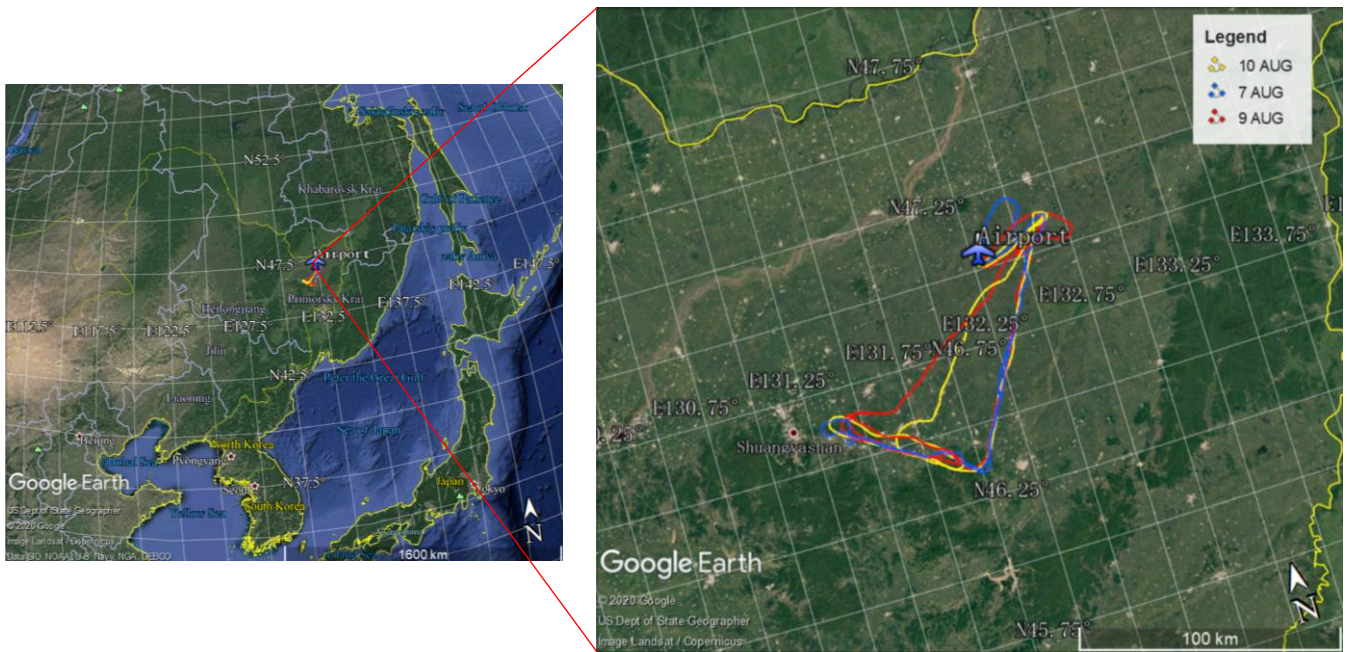
480 **Figure 3. Observation area for aircraft-based measurement of CO_2 and CH_4 over Jiansanjiang, Northeast China, and the flight paths on 7, 9, 10 August.**
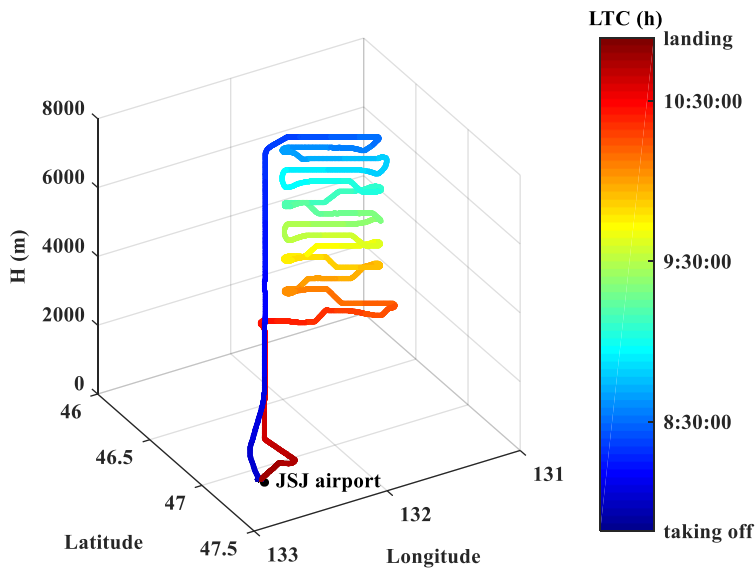
Figure 4. Trajectory on the 7 August, 2018 in Jiansanjiang. The color scale shows the progression of time (LTC), where blue
485 **represents the start time of the data profile, and red represents the end time.**
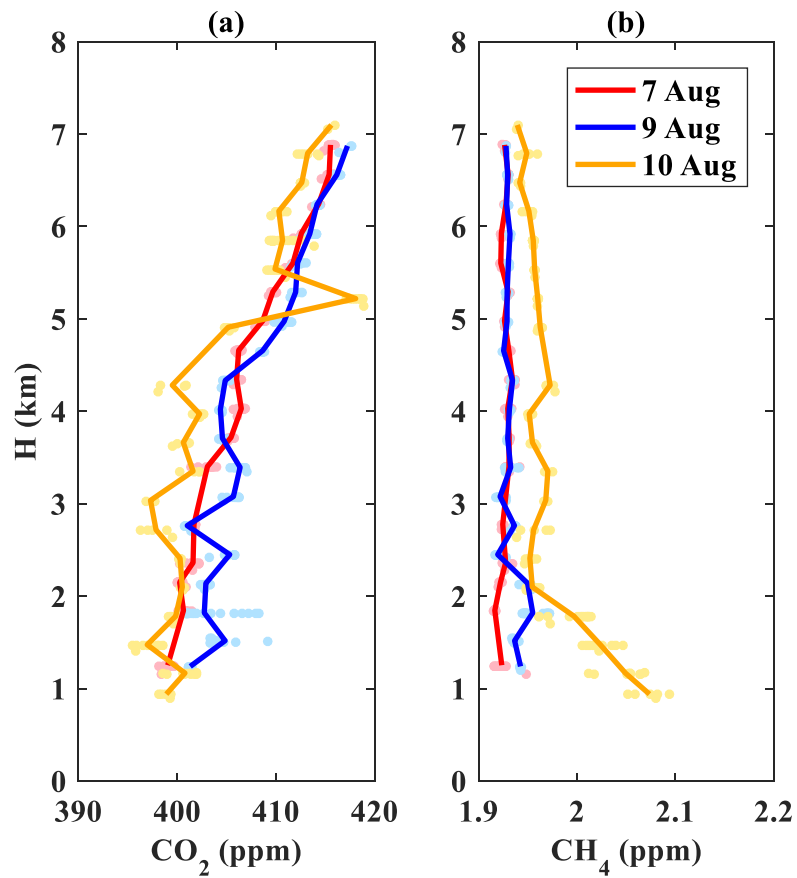
Figure 5 Vertical profiles of (a) CO₂ and (b) CH₄ observed on 7 (blue), 9 (red), and 10 (yellow), August, 2018, over Jiansanjiang measured in situ with aircraft. The aircraft-based in situ measurement data are indicated with dots, and averaged data for each flat flight stage are shown as lines.

490
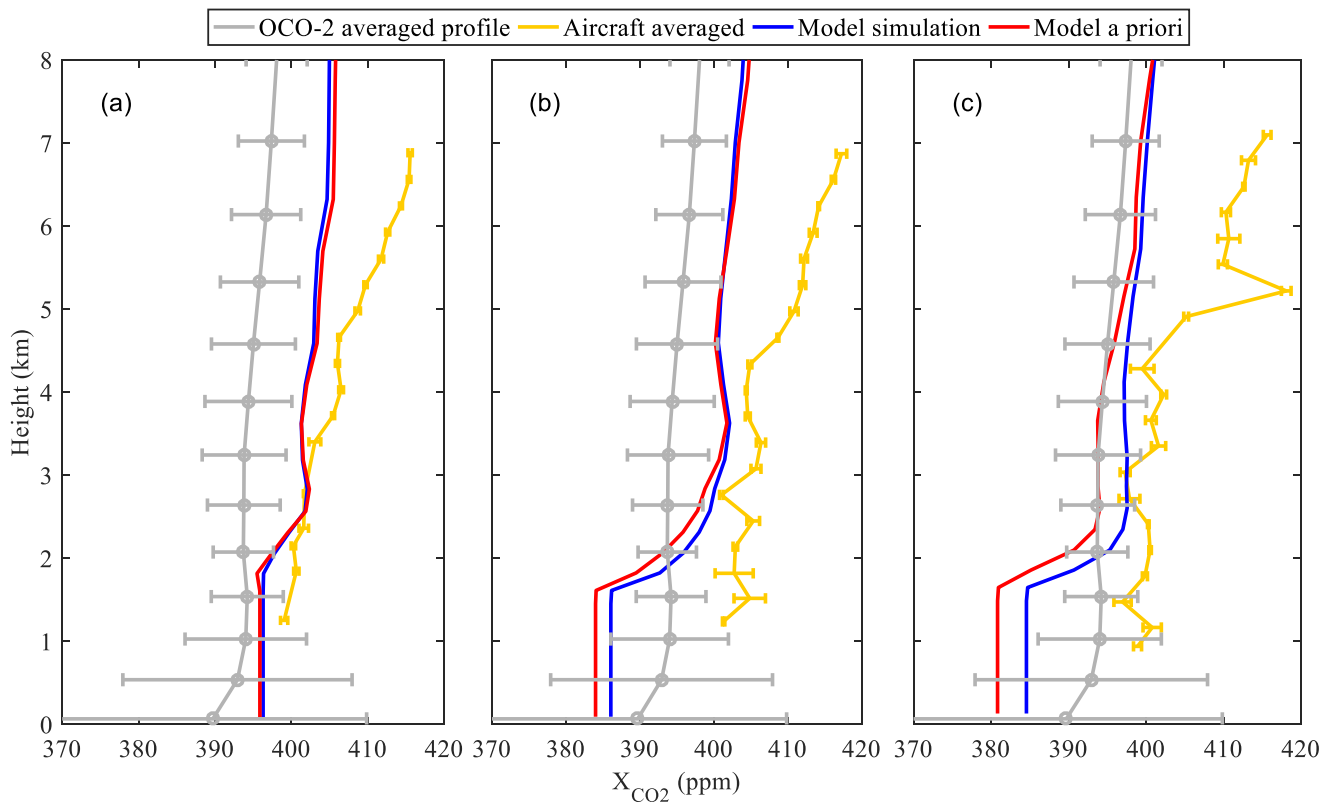
Figure 6. Comparison of aircraft measurements (in situ measurement data are shown by the yellow line) with 1 standard deviation (yellow bars) collected on (a) 7, (b) 9, and (c) 10, August Tan-Tracker (v1) data (blue line) and the a priori profile of it (red line) at the location of Jiansanjiang linearly interpolated to the observation times on (a) 7, (b) 9, and (c) 10 August, and the OCO-2 averaged profile (gray line) for the aircraft flight area from 5 August with 1 standard deviation (grey bars).
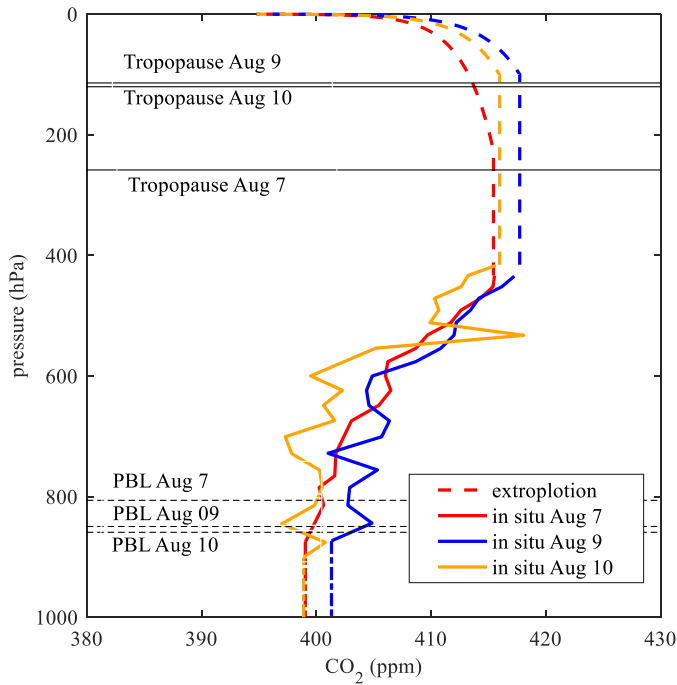
Figure 7. Extrapolated CO_2 **profiles observed on 7, 9 and 10 August, 2018, over Jiansanjiang by method (2). Red, blue, and yellow solid lines show the aircraft-based (in situ) data collected on 7, 9 and 10 August, respectively, averaged for each flat stage of the flight. Dotted lines show the extrapolated parts of the profiles, with colors corresponding to sampling dates in accordance with the solid lines. Black horizontal lines show the tropopause height from NCEP reanalysis data.**

500

Table 1 Details of the flight on each day.

Date	Flight Time (LTC)	Flight Altitude (m)
7 August, 2018	07:49:08-10:53:32	59-7205
9 August, 2018	07:50:19-10:45:57	61-7190
10 August, 2018	07:56:02-10:54:11	65-7104

Table 2. X_{CO_2} derived from aircraft on each observation day (7, 9 and 10 August) supplemented the aircraft profile by method (1). OCO-2 (V9r) X_{CO_2} were from 5 August, which was the closest time point of X_{CO_2} data from OCO-2 over Jiansanjiang to the observation period. Differences between aircraft X_{CO_2} and OCO-2 are shown in the fourth (ppm) and fifth (%) columns. The average difference and standard deviation are shown in the fifth row.

Date	Aircraft* (ppm)	OCO-2 (ppm)	Difference (ppm)	$\frac{\text{OCO-2-Aircraft}}{\text{Aircraft}} \cdot 100\%$ (%)
7 August, 2018	401.95		-5.04	-1.27
9 August, 2018	401.72	396.91	-4.81	-1.21
10 August, 2018	401.10		-4.19	-1.06
		Average (1σ)	-4.68(0.44)	-1.18(0.11)

*The effect of the average kernel was taken into consideration for OCO-2.

Table 3 The same as Table 2, but for method (2).

Date	Aircraft* (ppm)	OCO-2 (ppm)	Difference (ppm)	$\frac{\text{OCO-2-Aircraft}}{\text{Aircraft}} \cdot 100\%$ (%)
7 August, 2018	401.54		-4.63	−1.16
9 August, 2018	403.45	396.91	−6.54	−1.64
10 August, 2018	401.02		−4.11	−1.03
		Average (1σ)	−5.09 (1.28)	−1.28 (0.32)

*The effect of the average kernel was taken into consideration for OCO-2.

510

Table 4. Aircraft integration error budget of X_{CO_2} estimation for method (2). Errors in the three profiles from multiple error sources contributed to the calculation results of the integrated total column. There are four sources of error, similar to previously described error budgets (Wunch et al., 2017): the contribution from the aircraft profile itself, the contribution from the unknown surface to the bottom of the profile, the contribution from the upper troposphere and stratosphere, and error from the tropopause height.

Date	PBL errors (ppm)	Upper troposphere and stratosphere errors (ppm)	Tropopause height errors (ppm)
7 August, 2018	0.086	0.323	0.054
9 August, 2018	0.076	0.303	0.017
10 August, 2018	0.077	0.077	0.017
Average	0.079	0.234	0.029

515